

# Disruption of Macrodomain Protein SCO6735 Increases Antibiotic Production in *Streptomyces coelicolor*\*

Received for publication, February 13, 2016, and in revised form, August 31, 2016 Published, JBC Papers in Press, September 15, 2016, DOI 10.1074/jbc.M116.721894

Jasna Lalić<sup>‡1</sup>, Melanija Posavec Marjanović<sup>‡1</sup>, Luca Palazzo<sup>§1</sup>, Dragutin Perina<sup>‡</sup>, Igor Sabljic<sup>¶</sup>, Roko Žaja<sup>§||</sup>, Thomas Colby<sup>\*\*</sup>, Bruna Pleše<sup>‡</sup>, Mirna Halasz<sup>‡</sup>, Gytis Jankevicius<sup>§</sup>, Giselda Bucca<sup>‡‡</sup>, Marijan Ahel<sup>||</sup>, Ivan Matic<sup>\*\*</sup>, Helena Četković<sup>‡</sup>, Marija Luić<sup>¶</sup>, Andreja Mikoč<sup>‡2</sup>, and Ivan Ahel<sup>§3</sup>

From the <sup>‡</sup>Division of Molecular Biology, the <sup>¶</sup>Division of Physical Chemistry, and the <sup>||</sup>Division for Marine and Environmental Research, Ruđer Bošković Institute, Zagreb 10002, Croatia, the <sup>§</sup>Sir William Dunn School of Pathology, University of Oxford, Oxford OX1 3RE, United Kingdom, the <sup>\*\*</sup>Max Planck Institute for Biology of Ageing, D-50931 Cologne, Germany, and the <sup>‡‡</sup>School of Pharmacy and Biomolecular Sciences, University of Brighton, Huxley Building, Moulsecoomb, Brighton BN2 4GJ, United Kingdom

ADP-ribosylation is a post-translational modification that can alter the physical and chemical properties of target proteins and that controls many important cellular processes. Macrod domains are evolutionarily conserved structural domains that bind ADP-ribose derivatives and are found in proteins with diverse cellular functions. Some proteins from the macrodomain family can hydrolyze ADP-ribosylated substrates and therefore reverse this post-translational modification. Bacteria and *Streptomyces*, in particular, are known to utilize protein ADP-ribosylation, yet very little is known about their enzymes that synthesize and remove this modification. We have determined the crystal structure and characterized, both biochemically and functionally, the macrodomain protein SCO6735 from *Streptomyces coelicolor*. This protein is a member of an uncharacterized subfamily of macrodomain proteins. Its crystal structure revealed a highly conserved macrodomain fold. We showed that SCO6735 possesses the ability to hydrolyze PARP-dependent protein ADP-ribosylation. Furthermore, we showed that expression of this protein is induced upon DNA damage and that deletion of this protein in *S. coelicolor* increases antibiotic production. Our results provide the first insights into the molecular basis of its action and impact on *Streptomyces* metabolism.

Protein ADP-ribosylation is a reversible post-translational modification in which an ADP-ribose moiety from NAD<sup>+</sup> is transferred to a target protein. The covalent attachment of one ADP-ribose leads to mono-ADP-ribosylation, whereas the transfer of additional ADP-ribose molecules through *O*-glycosidic ribose-ribose bonds results in the synthesis of poly-ADP-

ribose (PAR)<sup>4</sup> polymers. The families that generate protein ADP-ribosylation, poly-ADP-ribose polymerases (PARPs), mono-ADP-ribosyltransferases, and certain sirtuins, in eukaryotes regulate a variety of cellular processes, such as DNA repair, transcription, regulation of centromere function, telomere length and aging, protein degradation, apoptosis, and necrosis (1–5). Poly-ADP-ribose glycohydrolase (PARG) is one of the proteins capable of removing ADP-ribosylation. PARG specifically cleaves PAR chains at *O*-glycosidic ribose-ribose bonds releasing ADP-ribose monomers or PAR oligomers, but it is unable to cleave the chemical bond between the proximal ADP-ribose unit and the modified proteins (6). Recent studies have demonstrated that a family of macrodomain proteins (MacroD1, MacroD2, and TARG1) can revert terminal, protein-proximal glutamate-linked mono-ADP-ribosylation (1, 7–9). TARG1, MacroD1/2, and PARG represent different subgroups within the macrodomain protein family (10). Macrod domains are ancient folds with high affinity for ADP-ribose binding (11, 12). These three macrodomain subgroups use the macrodomain for catalysis but with distinct mechanisms (reviewed in Ref. 1). Furthermore, an evolutionarily distinct protein that can catalyze the removal of the protein-proximal arginine-linked mono-ADP-ribosylation is a mono-ADP-ribosylhydrolase (ARH) 1 (13). Importantly, reversal of post-translational modification has been established as important in many cellular processes (7, 14, 15).

Although ADP-ribosylating bacterial toxins, which act by irreversibly modifying crucial host cell proteins, were discovered over 40 years ago (reviewed in Ref. 16), reversible mono-ADP-ribosylation and its role in signaling in bacteria is generally not well understood. Physiologically important, non-toxic mono-ADP-ribosylation has been extensively studied only in nitrogen-fixing bacteria *Rhodospirillum rubrum*, where the enzymes dinitrogenase reductase mono-ADP-ribose transferase and dinitrogenase reductase-activating glycohydrolase

\* This work was supported by Unity through Knowledge Fund Grant UKF 1B 2/13, European Research Council Grant 281739, Wellcome Trust Grant 101794, Cancer Research UK Grant C35050/A22284, and European Community's Seventh Framework Programme FP7/2007–2013 under BioStruct-X Grant 283570. The authors declare that they have no conflicts of interest with the contents of this article.

‡ Author's Choice—Final version free via Creative Commons CC-BY license.

<sup>1</sup> These authors contributed equally to this work.

<sup>2</sup> To whom correspondence may be addressed. Tel.: 385-14561115; Fax: 385-14561177; E-mail: mikoc@irb.hr.

<sup>3</sup> To whom correspondence may be addressed. Tel.: 44-01865285656; E-mail: ivan.ahel@path.ox.ac.uk.

<sup>4</sup> The abbreviations used are: PAR, poly-ADP-ribose; PARP, poly-ADP-ribose polymerase; PARG, poly-ADP-ribose glycohydrolase; RMSD, root mean square deviation; ARH, ADP-ribosylhydrolase; ART, ADP-ribosyltransferase; DraG, dinitrogenase reductase-activating glycohydrolase; PDB, Protein Data Bank; qRT-PCR, quantitative real time PCR; ANOVA, analysis of variance; MM, minimal medium; MMS, methyl methanesulfonate; ML, maximum likelihood.

## S. coelicolor Macrodomain Protein SCO6735

(DraG) regulate nitrogen fixation depending on nitrogen availability and energy status of the cell (17). Being the best characterized, bacterial DraG (homologue of human ARH1 and ARH3) is a representative of the group of arginine-specific ADP-ribosylhydrolases whose homologues are distributed across all three domains of life. Endogenous ADP-ribosylation has also been reported for some other bacteria, *Myxococcus xanthus* (18, 19), *Mycobacterium smegmatis* (20), *Bacillus subtilis* (21), and *Streptomyces* representatives (22–25), but little is known about its function in bacteria. Genomic evidence indicates that proteins involved in ADP-ribosylation processing are widespread among bacteria. Although PARP homologues are found rarely, PARG and other macrodomain protein homologues are found more often, suggesting that protein ADP-ribosylation is more common than previously thought (10). So far, the most evidence for intracellular endogenous protein ADP-ribosylation has been found in *Streptomyces* species. *Streptomyces* are soil bacteria well known for their complex life cycle, which includes morphological differentiation and production of secondary metabolites including antibiotics, anticancer drugs and immunosuppressors. In *Streptomyces griseus* and *Streptomyces coelicolor*, just like in other bacteria in which ADP-ribosylation has been studied, ADP-ribosylation patterns change with morphological differentiation and are related to changes in metabolic requirements (24, 26). However, almost nothing is known about transferases and hydrolases responsible for the reversible ADP-ribosylation in these organisms.

Thus far, no proteins have been identified that have the ability to reverse (hydrolyze) protein ADP-ribosylation in *Streptomyces* and most other bacterial organisms. Here, we analyzed the *S. coelicolor* genome and found a number of possible candidates, including homologues of human PARG and MacroD1, as well as an uncharacterized type of macrodomain protein, SCO6735. We have focused our research on SCO6735 because we could show that it encompasses a macrodomain evolutionarily close to the ALC1 (amplified in liver cancer)/TARG1 (terminal ADP-ribose protein glycohydrolase) macrodomain group. Here we determine the structure of SCO6735 and show that this protein hydrolyzes glutamate-linked protein mono-ADP-ribosylation. Furthermore, we show that depletion of SCO6735 leads to a significantly increased production of antibiotic actinorhodin in *S. coelicolor*.

## Results

**Putative ART and ARHs in *Streptomyces***—Our genomic analyses and homology searches predict the existence of only one potential ART in *S. coelicolor*, SCO5461, which confirms previous findings (27). SCO5461 is a highly diverged PARP homologue most similar to pierisins and mosquitocidal toxin and can modify guanosine and guanine mononucleotides *in vitro*, whereas its ability to directly modify proteins and *in vivo* substrates in general has not been clarified (28). SCO5461 is a secreted protein and is not found in *S. griseus* and most other *Streptomyces* species; thus it cannot be the major cellular protein ART in streptomycetes.

On the other hand, our analyses revealed a number of putative ADP-ribosyl protein hydrolases in *S. coelicolor* and other

streptomycetes, suggesting a lively ADP-ribosylation metabolism. We identified both DraG-like (SCO0086, SCO1766, SCO2028, SCO2029, SCO2030, SCO4435, and SCO5809) and macrodomain containing (SCO0909, SCO6450, and SCO6735) hydrolases. Two of three macrodomain proteins have predicted functions. The SCO0909 protein of *S. coelicolor* is a bacterial-type PARG, predicted to remove poly-ADP-ribosylation (6); whereas SCO6450 is a macrodomain protein predicted to remove mono-ADP-ribosylation, it is a homologue of the MacroD proteins, which are present in representatives from all three domains of life (10, 12). We focused our research on the third macrodomain protein, SCO6735. SCO6735 is a 161-amino acid protein with molecular weight of 17.4 kDa that belongs to an uncharacterized subgroup of macrodomain proteins. The orthologues of SCO6735 are less widely distributed than MacroD orthologues but still found in several bacterial phyla (Bacteroidetes, Firmicutes, and Planctomycetes). They are most frequent among Actinobacteria.

**SCO6735 Is a Macrodomain Protein That Groups into ALC1/TARG1 Branch**—We performed phylogenetic analysis using selected bacterial macrodomain proteins and human representatives of different macrodomain groups. Phylogenetic analyses showed that the SCO6735 groups into the ALC1/TARG1 branch (Fig. 1). ALC1 is a chromatin remodeler that uses its macrodomain to bind DNA damage induced poly-ADP-ribosylation (29). TARG1 removes PARP-dependent mono-ADP-ribosylation (7). SCO6735 shares 27% identity and 45% similarity with the human ALC1 macrodomain and 13% identity and 28% similarity with the TARG1 macrodomain.

Sequence alignment (Fig. 2) revealed conserved residues shared by SCO6735 and protein BT1257, from *Bacteroides thetaiotaomicron*, the most similar bacterial protein with a known crystal structure (unpublished, PDB code 2FG1). These two proteins share 48% identity and 62% similarity, and we assumed that the hypothetical protein BT1257 is likely the SCO6735 orthologue. It is worth noting that the residues important for ADP-ribose binding (Lys<sup>84</sup>) and hydrolytic activity (Asp<sup>125</sup>) of human TARG1 are not conserved in SCO6735 and BT1257 proteins.

**Biochemical Activity of SCO6735 Protein**—We wanted to assess whether SCO6735 has the ability to hydrolyze protein ADP-ribosylation, as has been demonstrated for some other macrodomain family members. First, we sought to determine whether the only predicted ART in *S. coelicolor*, SCO5461, can modify itself *in vitro*. Using an ADP-ribosyltransferase assay with [<sup>32</sup>P]NAD<sup>+</sup> as an ADP-ribose donor and the purified SCO5461ΔN34, we showed significant automodification activity. However, mono-ADP-ribosylated SCO5461ΔN34 was not a substrate for SCO6735, because we observed no decrease of the radioactive signal (Fig. 3A). We performed mass spectrometry analysis and identified aspartate 161 as a modification site on the auto-ADP-ribosylated SCO5461ΔN34. Next, we used a (heterologous) model substrate: mono-ADP-ribosylated PARP1 E988Q mutant, which is known to be modified mostly on glutamate residues (7). Using this substrate, we observed removal of radioactive signal suggesting enzymatic activity of SCO6735 against mono-ADP-ribosylated proteins modified on

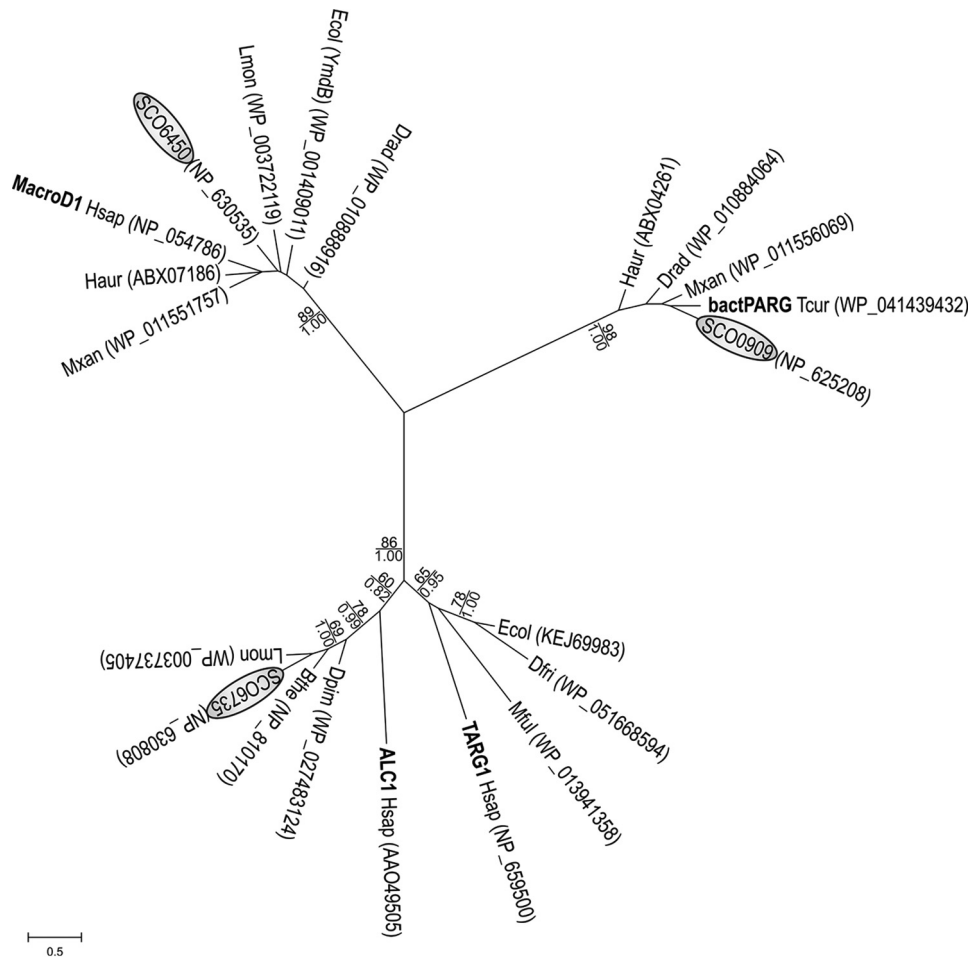


FIGURE 1. **Maximum likelihood phylogenetic tree illustrating the relationship between selected representative macrodomains.** Human proteins (*Hsap*) and bacterial PARG from *Thermomonospora curvata* (*Tcur*) are shown in bold type. *S. coelicolor* proteins are circled. Remaining macrodomain proteins were selected from the following bacterial species: *B. thetaioatomicron* (*Bthe*), *Deinococcus frigans* (*Dfri*), *Deinococcus pimensis* (*Dpim*), *D. radiodurans* (*Drad*), *E. coli* (*Ecol*), *Herpetosiphon aurantiacus* (*Haur*), *Listeria monocytogenes* (*Lmon*), *Myxococcus fulvus* (*Mful*), and *M. xanthus* (*Mxan*). Sequence accession numbers are given in parentheses. Bootstrap values ML (>60%) are given above the lines, and MCMC values are given (>0.6) below the lines. The scale bar indicates the genetic distance of the branch lengths.

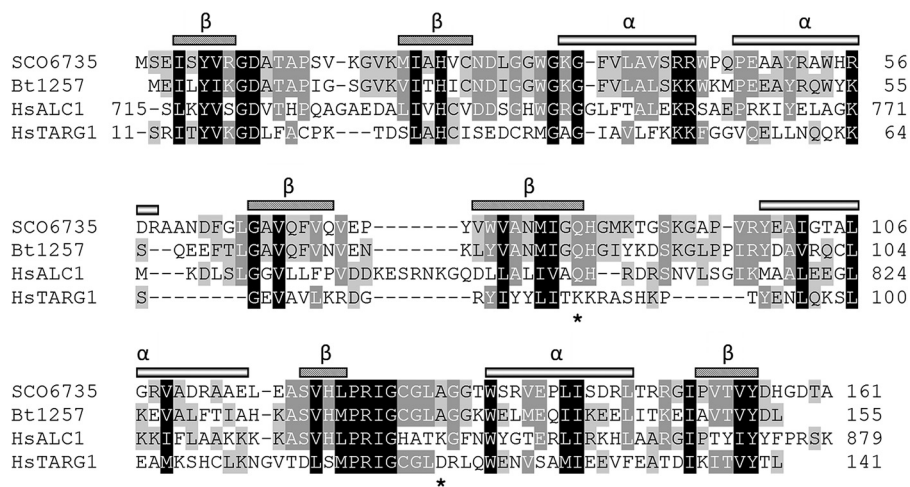
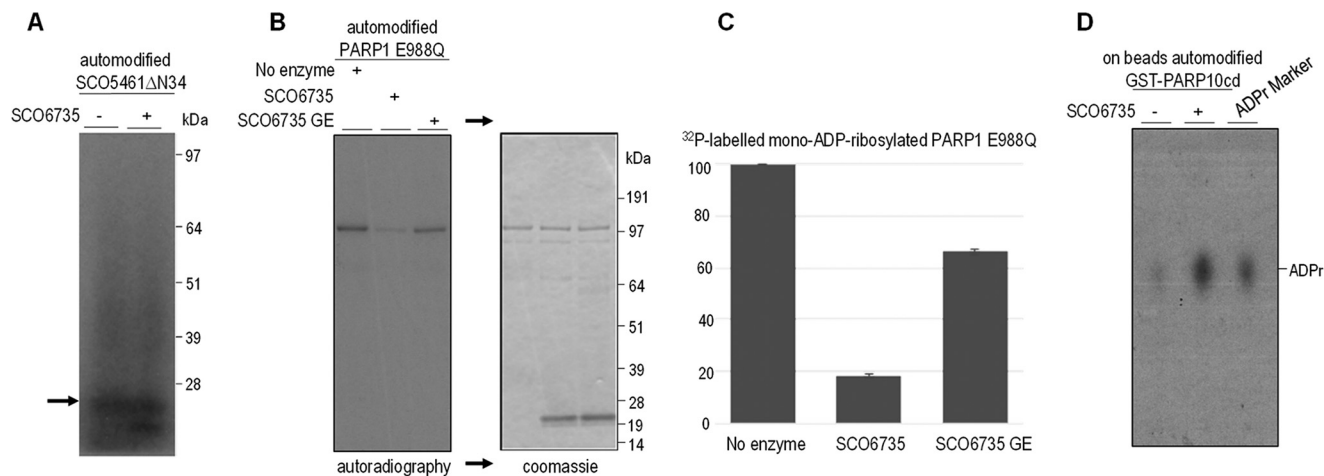


FIGURE 2. **Structure-based alignment of selected macrodomain protein sequences.** Designated secondary structure elements refer to SCO6735. Residues responsible for binding and hydrolysis of ADP-ribose in human TARG1 (Lys<sup>84</sup> and Asp<sup>125</sup>) are marked with asterisks.

glutamate residues (Fig. 3B). SCO6735 hydrolytic activity was partially abolished by a mutation of glycine 128 in glutamate (Fig. 3, B and C). To analyze the nucleotide product of SCO6735 activity, we used the automodified GST-PARP10cd as a sub-

strate and assayed the reaction products by thin layer chromatography (Fig. 3D). Our data showed that a major by-product of hydrolytic reaction is ADP-ribose, as seen for other macrodomain hydrolases (12). However, because the catalytic residues

## *S. coelicolor* Macrodomain Protein SCO6735



**FIGURE 3. Activity of SCO6735 protein.** *A*, activity of SCO6735 on  $^{32}\text{P}$ -automodified SCO5461 $\Delta$ N34 substrate. The arrow indicates the position of SCO5461 $\Delta$ N34 protein. *B*, activity of SCO6735 on automodified PARP1 E988Q protein. Recombinant PARP1 E988Q (0.5  $\mu\text{M}$ ) was automodified in presence of [ $^{32}\text{P}$ ]NAD $^{+}$  and treated or not with 1  $\mu\text{M}$  of SCO6735 or with 1  $\mu\text{M}$  of SCO6735 G128E mutant. *Right panel*, Coomassie staining of dried gel exposed in *left panel*. *C*, quantification of residual  $^{32}\text{P}$ -labeled ADP-ribose on PARP1 E988Q after treatment with buffer, SCO6735 or SCO6735 G128E mutant. The ratio between the intensity of each autoradiography band and correspondent intensity in Coomassie staining data are the means  $\pm$  S.D. of the values obtained in two independent experiments. *D*, TLC analyzing the by-products of incubation of GST-PARP10cd immobilized on beads with buffer or SCO6735. ADP-ribose marker was obtained treating recombinant wild type PARP1 with recombinant human PARG enzyme.

found in other macrodomain proteins such as TARG1 are not conserved in SCO6735 (Fig. 2), we conclude that the catalytic mechanism should be unique for the SCO6735 macrodomain subclass.

*Structure of SCO6735 Confirms Different Catalytic Residues Compared with TARG1*—To better understand the structure-function relationship of SCO6735 hydrolytic activity, we determined a high resolution (1.60 Å) crystal structure of this protein (Fig. 4). The structure of SCO6735 revealed highly conserved three-layered  $\alpha$ - $\beta$ - $\alpha$  sandwich macrodomain fold with a deep cleft that, by analogy with other macrodomain proteins, represents a putative ligand-binding site. A central six-stranded  $\beta$ -sheet contains a mixture of five parallel and one anti-parallel strand, and it is surrounded by four  $\alpha$ -helices. Structure alignment using PDBeFold (30) reveals many structural homologues within the PDB. Those most similar to SCO6735 are the structure of protein BT1257 from *B. thetaiotaomicron* (PDB code 2FG1; Z score of 14.4; RMSD 0.77) and the structure of human TARG1/C6orf130 (PDB code 4J5R; Z score of 9.4; RMSD 2.04) (7). Structural alignment of these three structures shows a high degree of similarity among them, with significant differences only in the loop regions.

The most pronounced difference is observed in the phosphate binding loop position. It was previously shown that, as for example in TARG1/C6orf130 protein, in both apo and complexed structures, the phosphate binding loop has the same position and encloses substrate within the active site (7). Surprisingly, in SCO6735 this loop is located far away ( $\sim 15$  Å) from the binding cleft (Fig. 4). Two amino acids from this loop, Gly $^{126}$  and Cys $^{127}$ , which were not well defined in the electron density maps, are omitted. B-factors in phosphate binding loop region are not significantly higher than B-factors of the surrounding amino acids, as also observed for TARG1/C6orf130 and BT1257 apo proteins, indicating similar flexibility of this loop in all three considered structures.

For TARG1/C6orf130 protein also NMR solution structures for both apo and ADP-ribose-bound complex are available in

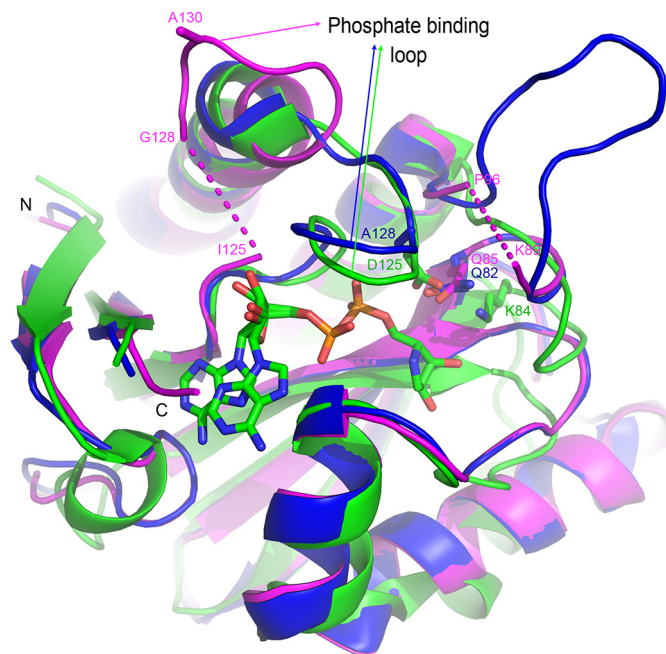


**FIGURE 4. Three-dimensional structure of SCO6735 (magenta) superimposed on a human TARG1/C6orf130 (PDB code 4J5R, green) and bacterial, *B. thetaiotaomicron* (PDB code 2FG1, blue) proteins.** Human protein is in complex with PARG inhibitor ADP-HPD. ADP-HPD, as well as amino acids important for ligand binding (Lys $^{84}$ ) and catalytic activity (Asp $^{125}$ ) and corresponding amino acids in bacterial structures (Gln $^{85}$  and Ala $^{130}$  in SCO6735 and Gln $^{82}$  and Ala $^{128}$  in BT1257) are shown in stick representation. Amino acids that could not be well defined in the electron density maps are omitted and shown by dashed line.

the literature (31). Interestingly, in none of the 20 final NMR conformers from apo and 20 from the complexed protein phosphate binding loop reaches a position so far away from the binding cleft as in SCO6735 structure. To check that the position of the phosphate binding loop in our structure is not a consequence of crystal packing, we carefully checked all contacts between amino acids composing the phosphate binding

Mtub recA	CCGACTTGTTCAGTGGCTGTCTCTAGTGT	-54- ATG	(X58485)
Scoe recA	GCCCATTTGTTCAGTGGCAGGCATTAGCGT	-43- ATG	(AL939125)
Scoe 6735	GGCCACTGTTCAGTGGTGGCCCGTACGGTGGCGTCATG		(AL939129)
Sliv 7081	GGCCACTGTTCAGTGGTGGCCCGTACGGTGGCGTCATG		(CP009124)
Sgri 991	GTGGCGTGTTCAGTGGCGGCCCGTACGGTGGCGTCATG		(AF009493)
Save 1676	GGCCACTGTTCAGTGGCAGTGCCTACGGTGGCGTCATG		(BA000030)
Sdav	GGCCACTGTTCAGTGGCAGCGCCCTACGGTGGCGTCATG		(HE971709)
Sful 6504	GCCCGCTGTTCAGTGGCGGCCCGTACGGTGAAGCCATG		(CP005080)
Consensus	CTGTTCAGTG	TAcgGT	

**FIGURE 5. Alignment of the RecA-NDp promoter sequences of *Mycobacterium tuberculosis* (Mtub) and *S. coelicolor* (Scoe) recA genes with SCO6735 and its orthologues in other *Streptomyces* species.** Sliv, *S. lividans*; Sgri, *S. griseus*; Save, *Streptomyces avermitilis*; Sdav, *Streptomyces davaensis*; Sful, *Streptomyces fulvissimus*. Putative promoter sequences are boxed, and the (potential) transcription start sites are underlined. The numbers indicate the distance to the starts of translation with respect to the shown sequences. GenBank™ accession numbers for the sequences are given in parentheses.

loop and surrounding symmetry equivalent molecules. We found out that there is only one hydrogen bond (Leu<sup>129</sup> N-H...O<sup>81B</sup> Asp<sup>156</sup>). There are no polar amino acids in the phosphate binding loop (<sup>123</sup>RIGCGLAGG<sup>133</sup>), except for the first arginine residue, suggesting that it is not very likely that electrostatic contacts are responsible for phosphate binding loop configuration. The same is valid for hydrophobic interactions caused by a lack of hydrophobic residues in this loop.

A structural comparison shows that the catalytic residues of TARG1 (Lys<sup>84</sup> and Asp<sup>125</sup>) are not conserved in SCO6735 and BT1257 (replaced by Gln and Ala, respectively), additionally confirming that these proteins utilize different catalytic mechanism. Up to now we were not able to obtain the SCO6735 structure with bound ADP-ribose.

**SCO6735 Is UV-inducible**—To further understand the physiological function of SCO6735, we analyzed its promoter region to get an insight into the transcriptional regulation of the gene product. Strikingly, in the intergenic region, upstream of the SCO6735 gene, we found a highly conserved RecA-NDp type of promoter. Because this type of promoter precedes numerous genes involved in the DNA damage response in *Actinomyce-tales* (32, 33), it strongly suggested connection of SCO6735 macrodomain protein with DNA damage response in *Streptomyces*. Furthermore, the RecA-NDp promoter is also found upstream of SCO6735 homologues in several other *Streptomyces* species (Fig. 5).

We tested whether the SCO6735 gene is inducible by the SOS response. Regulation of SCO6735 gene expression upon DNA damage was analyzed using UV light as a DNA-damaging agent. Using a PCR analysis (Fig. 6A), we observed that expression of the SCO6735 gene in the *S. coelicolor* WT strain was notably increased after UV irradiation. To quantify this observation, we performed quantitative real time PCR analysis using a gene for 16S rRNA as an invariant endogenous control and recA gene as a positive control. Quantitative real time PCR (Fig. 6B) confirmed that the expression of the SCO6735 gene was significantly (5-fold) increased (two-tailed *t* test, *p* = 0.0337) after DNA damage caused by UV irradiation, thus implicating involvement of the SCO6735 protein in the DNA damage response.

**Disruption of the SCO6735 Gene and Mutant Phenotype**—The DNA damage response promoter suggested that SCO6735 protein may have a DNA repair function, so we decided to inactivate the gene encoding SCO6735 protein in *S. coelicolor* and

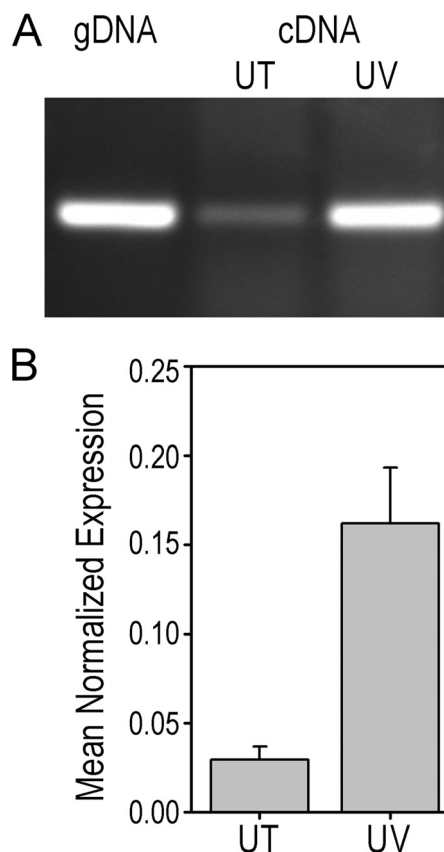


**FIGURE 6. Expression of SCO6735 gene is up-regulated upon DNA damage.** cDNA from untreated (UT) and UV-irradiated (200 J m<sup>-2</sup>) mycelium (UV) of *S. coelicolor* wild type strain was used as a template for PCR (A) and qRT-PCR analyses (B). *S. coelicolor* genomic DNA (gDNA) was used as a control template in PCR analysis. The data represent the mean values from three independent experiments. The error bars represent standard error of the mean.

analyze the phenotypes. We used the REDIRECT gene replacement procedure (34) to replace the SCO6735 gene from the *S. coelicolor* WT strain by an apramycin resistance cassette as described under “Experimental Procedures.” Disruption of the SCO6735 gene was confirmed by PCR, Southern hybridization of genomic DNA and qRT-PCR (data not shown). The deletion mutant used for further analysis was named *S. coelicolor* Δ6735.

To analyze whether the *S. coelicolor* Δ6735 strain exhibits sensitivity to DNA damage, we performed assays with two different mutagens. Spores of *S. coelicolor* WT and SCO6735 deletion mutant were irradiated with UV light (up to 300 J m<sup>-2</sup>) and treated with methyl methanesulfonate (MMS; up to 13 μg/μl) as described. Survival rates were determined as shown in Fig. 7. We did not notice significant differences in the survival rate between *S. coelicolor* WT and *S. coelicolor* Δ6735 strains after UV or MMS treatment. The absence of a DNA damage-sensitive phenotype could be a consequence of redundant pathways that can efficiently repair damage produced by UV-light and MMS. Alternatively, it is quite possible that SCO6735 is not directly involved in DNA repair.

To explore other phenotypes, we assessed the growth of *S. coelicolor* Δ6735 on various culture media that might reveal changes in secondary metabolism. When grown on minimal medium, *S. coelicolor* Δ6735 showed a “blue phenotype,” sug-

## *S. coelicolor* Macrodomain Protein SCO6735

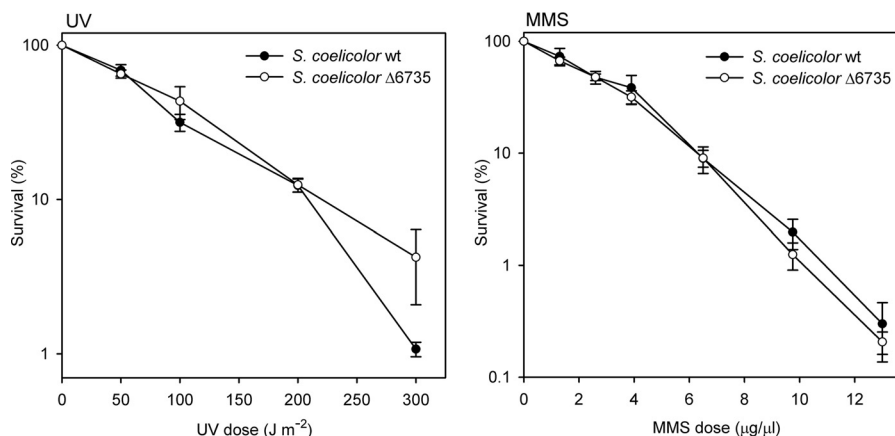


FIGURE 7. **UV and MMS sensitivity of the *S. coelicolor* Δ6735 mutant compared with wild type.** The data represent the mean values from three independent experiments. The error bars represent standard error of the mean.

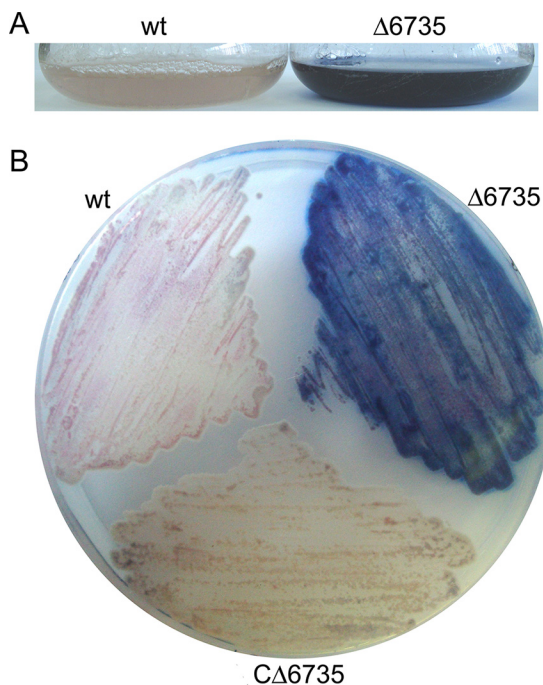


FIGURE 8. **Blue phenotype of *S. coelicolor* Δ6735 mutant in liquid (A) and on solid (B) minimal medium compared with wild type and complementation strain (CΔ6735) phenotypes.**

gesting accelerated and higher production of antibiotic actinorhodin when compared with the wild type strain (Fig. 8). To confirm that this phenotype is specifically due to disruption of SCO6735 function, we performed complementation analysis using ectopically expressed SCO6735. The SCO6735 gene, together with its RecA-NDp promoter region, was cloned into the site-specific integrating vector pMS82 and integrated into the *S. coelicolor* Δ6735 strain genome. The complementation strain, named *S. coelicolor* CΔ6735, showed reversion of the blue phenotype, indicating that the observed phenotype is a consequence of SCO6735 gene inactivation (Fig. 8).

**Quantification of Actinorhodin Production in *S. coelicolor* Δ6735 Mutant**—Because the SCO6735-deficient strain showed a conditional effect on the production of antibiotic actinorhodin, we quantified the level of actinorhodin in *S. coelicolor* WT, SCO6735-deficient, and complementation strains.

All strains were grown in liquid minimal medium for 5 days, and aliquots taken every 24 h were used to quantify intracellular and extracellular actinorhodin content. Pooled data for all days and measurements showed (Fig. 9) that actinorhodin levels in SCO6735-deficient mutant increased over time and were significantly higher compared with both the WT and complementation strains. *S. coelicolor* Δ6735 produced significantly more intracellular actinorhodin than both of the reference genotypes, on average 6.5 times more than the wild type and 8.72 times more than complementation strain (one-way ANOVA,  $p < 0.0001$ ). Similar results were observed for the extracellular actinorhodin. The *S. coelicolor* Δ6735 strain produced on average 5.57 and 10.3 times more extracellular actinorhodin than the wild type and complementation strain, respectively (one-way ANOVA,  $p < 0.0001$ ). Wild type and the complementation strain did not significantly differ in the levels of either intracellular (one-way ANOVA,  $p = 0.9232$ ) or extracellular (one-way ANOVA,  $p = 0.8636$ ) actinorhodin.

**Deregulation of Actinorhodin-related Gene Expression in *S. coelicolor* Δ6735 Mutant**—Using qRT-PCR, we analyzed whether deficiency in SCO6735 protein influences expression of genes responsible for actinorhodin biosynthesis and regulation. Biosynthesis of the polyketide antibiotic actinorhodin is determined by ~20 genes organized in five transcription units within the *act* gene cluster (35) dependent on the ActII-ORF4 protein, which binds to sequences in the target promoters (36). Two genes from the actinorhodin biosynthesis cluster that we included in our analysis were actinorhodin cluster activator protein (*actII-ORF4*) gene SCO5085 and  $\alpha$ -subunit of actinorhodin polyketide  $\beta$ -ketoacyl synthase (*actI-ORF1*) gene SCO5087. Expression of these genes was analyzed in the *S. coelicolor* WT strain, SCO6735-deficient mutant, and the complementation strain. The strains were grown in liquid minimal medium for 5 days, and total RNA was isolated from the samples taken every 24 h. Our results (Fig. 10) confirmed that expression of both genes involved in actinorhodin biosynthesis was significantly increased in SCO6735-deficient strain compared with WT strain (two-tailed *t*-tests,  $p > 0.0148$  and  $p > 0.0001$  for SCO5085 and SCO5087, respectively). Wild type and the complementation strain did not significantly differ in the

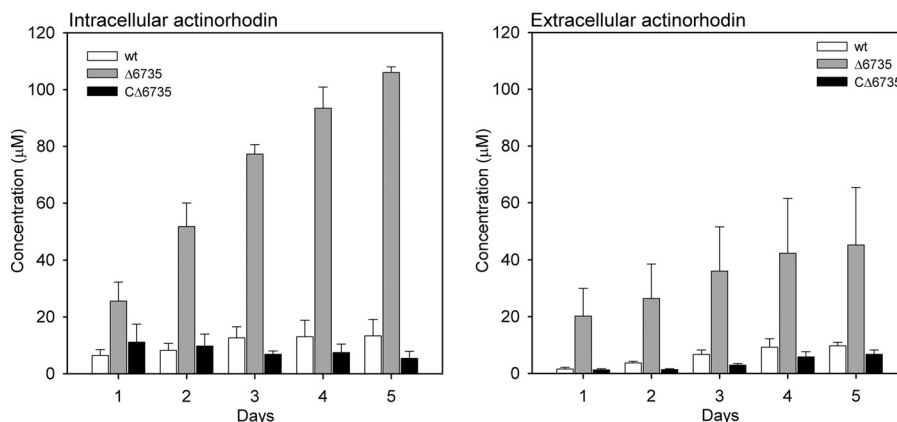


FIGURE 9. The content of intracellular and extracellular actinorhodin in *S. coelicolor* WT, Δ6735 mutant, and complementation strain (CΔ6735) over 5 days of growth in minimal medium. The data represent the mean values from three independent experiments. The error bars represent standard error of the mean.

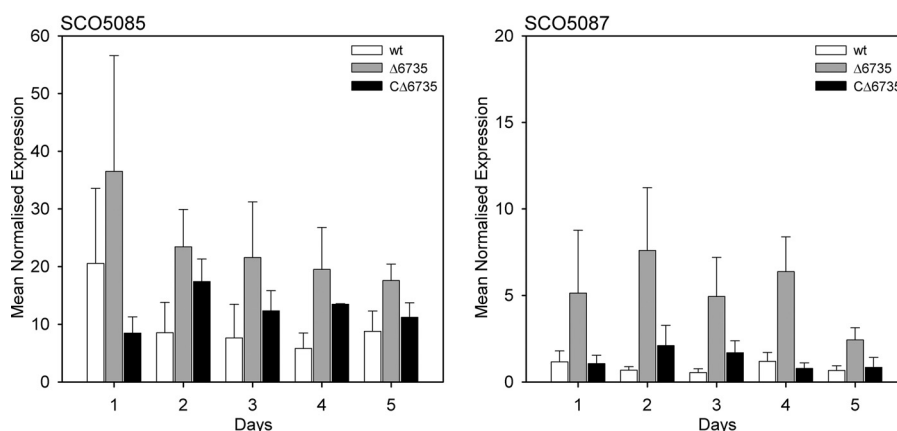


FIGURE 10. Quantitative real time PCR analysis of genes involved in the biosynthesis of actinorhodin, SCO5085, and SCO5087 in *S. coelicolor* Δ6735 mutant, wild type and complementation strain. Samples for RNA isolation were taken during the 5 days of growth in minimal medium. The data represent the mean values from three independent experiments. The error bars represent standard error of the mean.

levels of both SCO5085 and SCO5087 gene expression (two-tailed *t*-tests,  $p = 0.6974$  and  $p > 0.6579$ , respectively).

## Discussion

Very little is known about bacterial reversible ADP-ribosylation, with the exception of the role in nitrogen fixation in *Rhodospirillum* and *Azotobacter* species (17). Scattered evidence suggests that ADP-ribosylation in bacteria is much more common in regulating important cellular pathways, e.g. development and possibly mediating cell-cell contact in *M. xanthus* (18, 19), differentiation process in *B. subtilis* (21), and differentiation and secondary metabolism in *Streptomyces* (22, 37). Finally, here we suggest the possible involvement of the de-ADP-ribosylation process in the control of *S. coelicolor* antibiotic production. However, a direct role of SCO6735 protein and de-ADP-ribosylation reactions in this process remains to be experimentally verified. Transferases and hydrolases involved in ADP-ribosylation processes remain largely uncharacterized in bacteria. Genomic evidence indicates that only a small number of bacterial species possess all genes encoding proteins essential for a functional PAR metabolism, although there is no evidence that functional PAR metabolism really exists in bacteria. These genes were possibly acquired through horizontal gene transfer (6, 38), and bacteria might have evolved to use

PARG as counteracting factor of the potentially harmful ADP-ribose/PARG present in the environment. PARGs are present in a scattering of bacteria. In *Deinococcus radiodurans* PARG is one of the highly induced proteins upon DNA damage caused by UV light (39). Protein mono-ADP-ribosylation is predictably more common in bacteria (10), where homologues of MacroD proteins are the most abundant representatives. Macrodomain protein YmdB from *Escherichia coli* seems to be a multifunctional protein that regulates RNase III activity and modulates bacterial biofilm formation (40).

Current genomic data suggest that ADP-ribosylation should be prominent in *Streptomyces*, with one possible ART and many ARHs. Even though ADP-ribosylation has been noted in *Streptomyces* more than 20 years ago, there is still very little mechanistic understanding of how ADP-ribosylation is regulated in these organisms. So far, only one ADP-ribosyltransferase has been identified in *Streptomyces*: SCO5461 protein. In accordance with structural similarity with two toxic ADP-ribosyltransferases, pierisins and mosquitocidal toxin, SCO5461 has been described as a DNA-modifying exotoxin, and its ADP-ribosylating activity toward N2 amino groups of guanine nucleosides, as well as mononucleotides, has been shown (28). Sziráč *et al.* (37) have shown that disruption of SCO5461 leads

## *S. coelicolor* Macrodomain Protein SCO6735

to conditional pleiotropic phenotype characterized by morphological differentiation and antibiotic production defects. In addition, the same authors showed that deficiency in SCO5461 leads to a minor effect in protein ADP-ribosylation patterns; however, the question remained whether the effect was direct (37). Here we confirmed auto mono-ADP-ribosylating activity of the SCO5461 protein *in vitro*, but its specific protein targets are yet to be discovered. Several identified ADP-ribosylated proteins in *S. coelicolor* suggested a connection between protein ADP-ribosylation and the regulation of metabolic requirements of the cells (25, 41). SCO5461 is not conserved across the *Streptomyces* species (including *S. griseus*), suggesting that the major protein ADP-ribosyltransferases in *Streptomyces* are yet to be uncovered.

Surprisingly, there is evidence of a much larger number of potential ADP-ribose protein hydrolases in *S. coelicolor*. Seven of them are uncharacterized DraG homologues (SCO0086, SCO1766, SCO2028, SCO2029, SCO2030, SCO4435, and SCO5809), whereas three are macrodomain proteins (SCO0909, SCO6450, and SCO6735), representing three different groups of macrodomain superfamily. Although in eukaryotes macrodomains exist as compositions with other domains forming functionally complex proteins like ALC1, PARP9, and macroH2A1 (29, 42, 43), macrodomain proteins in bacteria are usually stand-alone proteins. Our preliminary results indicate that SCO6450, just like its human homologue MacroD1, indeed possesses enzymatic activity capable of removing ADP-ribose from mono-ADP-ribosylated protein. The SCO0909 protein is a bacterial-type PARG. Bacterial-type PARGs are much shorter than the proteins in human and higher eukaryotes and encompass only the PARG catalytic domain but are highly active and specific in hydrolyzing PAR *in vitro* (6). Our data showed that SCO6735 removes ADP-ribosylation from glutamate residues but does not reverse ADP-ribosylated SCO5461. This is further evidence that the relevant transferase(s) in *Streptomyces* are yet to be discovered. SCO6735 and its orthologue BT1257 represent a new subgroup of macrodomain proteins with a catalytic mechanism that is different from any known macrodomain proteins.

Our results, in accordance with previous findings, suggest the potential role of ADP-ribosylation in the regulation of metabolism (antibiotic production) in *Streptomyces*, whereas for the first time we have shown the possible involvement of ADP-ribosylation in response to DNA damage in *Streptomyces*. Involvement of ADP-ribosylation in the repair of DNA damage is well known and has been demonstrated in detail in eukaryotes (44, 45). A few lines of evidence suggest that ADP-ribosylation could also be involved in the DNA damage response in prokaryotes. In *M. smegmatis*, ADP-ribosyltransferase Arr was up-regulated in response to various stresses, including DNA damage (46). In *D. radiodurans*, PARG was up-regulated upon UV-induced DNA damage, pointing out that degradation of PAR could be more ancient than was initially considered (39). Gene SCO6735 is under control of the RecANDp promoter, and its expression is also up-regulated upon UV-induced DNA damage. Nevertheless, using two different mutagens (UV light and MMS), we were not able to show significant DNA damage-sensitive phenotype of the SCO6735-deficient

mutant. This may not be unexpected given that *Streptomyces* possess multiple DNA repair systems that transcend bacterial systems and are closer to those of lower eukaryotes (47, 48).

To conclude, we believe our findings will help to understand ADP-ribosylation processes in *Streptomyces* (and bacteria in general) and establish *Streptomyces* as an important model to study bacterial ADP-ribosylation. Our data confirm that ADP-ribosylation in *Streptomyces* could be even more widely utilized than initially thought. For example, we uncovered possible involvement of de-ADP-ribosylation process in the control of antibiotic production and demonstrated a potential link between ADP-ribosylation and the DNA damage response.

### Experimental Procedures

**Bacterial Strains, Culture Conditions, and Plasmids**—*S. coelicolor* M145 strain, a derivative of the wild type strain A3(2) lacking plasmids SCP1 and SCP2, was a generous gift from Prof. M. Bibb and was used in this study as a wild type strain (49). *S. coelicolor* strains were grown at 30 °C in liquid medium: complete regeneration medium (50) and minimal medium (MM) (49), and on solid media: mannitol soya flour, tryptic soy broth (TSB) (Difco), nutrient agar (Difco), and MM. For actinorhodin quantification and actinorhodin-related gene expression quantification, spores of different *S. coelicolor* strains were inoculated into complete regeneration medium and grown for 24 h. The next day, mycelia were washed in MM and continued incubation in 50 ml of MM for 5 days at 30 °C and 250 rpm. Every 24 h, aliquots were taken for the further analyses.

*E. coli* XL1-Blue (New England Biolabs) was used for all genetic manipulations. *E. coli* BL21(DE3) (Stratagene) was used for gene overexpression. Strains *E. coli* BW25113/pIJ790 and ET12567/pUZ8002 and cosmid St5F2A (51) used for gene disruption by REDIRECT technology (34) were obtained from the John Innes Centre (Norwich, UK). *E. coli* strains XL1-Blue and BL21(DE3) were grown in LB liquid and solid medium at 37 °C, whereas strain BW25113/pIJ790 at 30 °C until the loss of the plasmid with temperature sensitive origin of replication was needed. When necessary, the media were supplemented with antibiotics to the following concentrations: 100 µg/ml of ampicillin, 50 µg/ml of apramycin, 25 µg/ml of chloramphenicol, 50 µg/ml of kanamycin, 25 µg/ml of nalidixic acid, or 50 µg/ml of hygromycin. All antibiotics were purchased from Sigma-Aldrich. Plasmid pET15b (Novagen) was used for gene overexpression and *Streptomyces*-specific integrative vector pMS82 (52) for complementation analysis (a generous gift from Prof. M. Smith).

**Gene Cloning, Mutagenesis, Overexpression, and Protein Purification**—*S. coelicolor* genomic DNA was isolated as described (49) and used for PCR amplification of the gene encoding SCO6735 protein (NCBI, gene identifier 1102174) with primers 6735F (CGGTGGCCATATGTCGGAGAT-CAGCTATGTCC) and 6735R (GAGCCGCGGATCCCC-TAGGCGGTGTCCCCG) that contain NdeI and BamHI restriction sites. PCR product was digested with the same restriction enzymes and cloned into pET15b. Specific point mutation was introduced using this plasmid construct, mutant primers 6735GEF (CCGCATAGGCTGCGAGCTGGCCG-GCGGCAC) and 6735GER (GTGCCGCCGCCAGCTCG-CAGCCTATGCGG) and the asymmetric overlap extension

PCR method for site-directed mutagenesis (53). The gene encoding SCO5461 protein (NCBI, gene identifier 1100901) was amplified using primers 5461F (GCCGCCATATGC-CGTCCGGCTGCCCCGCAAG) and 5461R (GAGCCAG-GATCCCCGGTGTCTAGTGCCAGGGC) and cloned into pET15b. These primers were designed to skip the first 102 nucleotides (that correspond to the first 34 amino acids spanning the predicted transmembrane region). The resulting plasmid constructs were verified by sequencing and introduced into *E. coli* BL21(DE3). Overexpression of the recombinant SCO6735 gene in the 2-liter culture was induced with 0.1 mM isopropyl  $\beta$ -D-thiogalactopyranoside at  $A_{600} = 0.8$  and continued at 16 °C overnight. Overexpression of the recombinant SCO5461 gene in the 500-ml culture was induced with 0.8 mM isopropyl  $\beta$ -D-thiogalactopyranoside at  $A_{600} = 0.8$  and continued at 30 °C for the next 3 h. Bacteria were harvested by centrifugation, resuspended in buffer P (25 mM Tris-HCl, pH 7.5, 500 mM NaCl) containing 10 mM imidazole and 1 mg/ml lysozyme and disrupted by sonication ( $5 \times 30$  s). After removing cellular debris by centrifugation at  $13,000 \times g$  for 30 min, His-tagged recombinant proteins were purified by TALON metal affinity chromatography (Clontech). TALON resin was washed two times in buffer P containing 10 and 20 mM imidazole, whereas elution was performed with the same buffer containing 200 mM imidazole. Purified protein fractions were pooled, desalted on PD10 columns (GE Healthcare), and stored in buffer containing 25 mM Tris-HCl (pH 7.5), 50 mM NaCl, 1 mM EDTA, 1 mM DTT and 10% glycerol (v/v). PARP1 E988Q mono-mutant was purified as described previously (7). Recombinant PARG was purified as described previously (54). pGEX-4T1 GST-PARP10cd (amino acids 818–1025) was purified as previously described (55) with slight modifications. Briefly, after binding of GST-tagged PARP10 on glutathione-Sepharose beads (GE Healthcare), the protein was extensively washed in lysis buffer and equilibrated in PARP10 reaction buffer (50 mM Tris-HCl, pH 7.5, 75 mM KCl, 4 mM MgCl<sub>2</sub>, 0.25 mM DTT). Protein was kept on beads for the automodification reaction.

**Gene Disruption and Complementation**—Gene disruption was done by replacing the entire coding region of SCO6735 gene with the apramycin resistance cassette using the REDIRECT PCR targeting system (34). The SCO6735 disrupting cassette was generated by PCR using plasmid pIJ773 as a template and specific primers 6735F (GGGGCCACTGT-CAGTGGTGGCCCCGTACGGTGGCGTTCATGattccggggatc-cgtcgacc) and 6735R (ACGAACGACGTGCACGAGCACT-GAGCCGCGGACGGCCTAtgtaggctggagctgcttc), which match the sequences adjacent to the SCO6735 coding region ending in start/stop codons (capital letters) and right/left end of the disruption cassette (lowercase letters). PCR product was used to transform *E. coli* strain BW25113/pIJ790 containing *S. coelicolor* cosmid St5F2A (carrying the SCO6735 gene). After recombination, a strain with mutated cosmid was selected, cosmid was isolated, introduced into *E. coli* ET12567/pUZ8002 to avoid methyl-sensing restriction system, and transferred to *S. coelicolor* by conjugation. Exconjugants were screened for double cross-over recombinants and verified by PCR (using primers T6735F: GTGCTGCTGCTGCCCGTG and T6735R: CTGTTCCAGC-CGTCGAAG), genomic Southern analysis, and qRT-PCR.

For the complementation analysis SCO6735 gene was amplified by PCR using *S. coelicolor* genomic DNA as a template and specific primers with introduced SpeI and EcoRV restriction sites (6735SpeI: TCGCGCACTAGTCCGGGCAGGAACGG-CCGGCGCC and 6735EcoRV: GTGCACGATATCTGAG-CCGCGGACGGCCTAGGC) and cloned into the site-specific integrating vector pMS82 carrying *attP-int* locus derived from the phage  $\phi$ BT1 (52). Resulting plasmid construct (pMS82-SCO6735) was verified by sequencing, introduced into *S. coelicolor*  $\Delta$ 6735 strain by conjugation, and integrated into the phage  $\phi$ BT1 *attB* integration site via double cross-over.

**Actinorhodin Quantification**—Intracellular and extracellular actinorhodin contents were quantified following the protocol (56) with a single modification using 1 M NaOH instead of 1 M KOH. Intracellular actinorhodin content was quantified from 1-ml culture pellet, whereas supernatant was used to quantify the extracellular  $\gamma$ -actinorhodin. Bacteria were lysed with NaOH, and actinorhodin was precipitated with HCl. Actinorhodin pellet was suspended in 1 M NaOH, and  $A_{640}$  was measured. Concentrations were calculated according to the Lambert-Beer's law using molar extinction coefficient of the pure actinorhodin in NaOH ( $\epsilon_{640} = 25,320$  liters mol<sup>-1</sup> cm<sup>-1</sup>). All quantifications were done on three independent biological replicates of each of the genotypes.

**RNA Isolation and Genes Expression Quantification by qRT-PCR**—The total RNA was isolated from 100-mg culture pellets using the RNeasy mini kit (Qiagen) following the user manual. Genomic DNA was degraded on column using DNase I provided with the same kit. The quality of isolated RNA was examined by agarose gel electrophoresis and spectrophotometrically, whereas the absence of DNA was confirmed by PCR. 1  $\mu$ g of total RNA isolated from each sample was subjected to reverse transcription using the high capacity cDNA reverse transcription kit (Applied Biosystems). *S. coelicolor* 16S rRNA housekeeping gene was used for normalization (57). The SCO6735 gene was used as a negative control for the SCO6735 knock-out mutant. The following primers were used in qRT-PCR analyses: SCO5085F, GTAATTTTCGCATCCGCTGAAC; SCO5085R, GGAGATTCGATACGATTCCAG; SCO5087F, GAAGGAGCTGTTCCGATTGAAG; SCO5087R, AGGTG-AGCAGTTCAGAA; 16SF, GCGGCGGAGCATGTGGCTTA; 16SR, CACCTGTACACCGACCACAA; RT6735F, GGCTGGGGCAAGGGCTTCGT; and RT6735R, GCGCCG-AGACCGAAGTCGTT.

All primer pairs were tested *a priori*, and their efficiency was measured as described (58) and used for the analyses of mean normalized expression (58). Quantitative real time PCRs were performed in 10- $\mu$ l volume using SYBR Green PCR Master Mix (Applied Biosystems), 900 nM primers (each), and 1.5  $\mu$ l of cDNA. The thermal profile consisted of 10-min initial denaturation at 95 °C followed by 40 cycles of 15 s at 95 °C and 1 min at 60 °C. Each RNA sample was quantified two times in independent experiments. Amplifications were done using the ABI PRISM Sequence Analyzer 7300 (Applied Biosystems). Quantification results were examined using SDS7300 software version 1.4 (Applied Biosystems). Statistical analyses were done using R version 3.2.1. Mean normalized expression (MNE) of

## S. coelicolor Macrodomain Protein SCO6735

the genes whose deregulation was tested by qRT-PCR was calculated using the formula as described (58),

$$\text{MNE} = 10^2 \frac{\epsilon R_{\overline{C}_{T(R)}}}{\epsilon \overline{C}_{T(G)}} \quad (\text{Eq. 1})$$

where  $\epsilon$  is the efficiency of the primer pair amplifying either the reference (*i.e.* housekeeping) gene ( $R$ ) or the gene tested for the deregulation ( $G$ ), and  $\overline{C}_{T}$  is the mean value of threshold cycle in qRT-PCR. All quantifications were done on at least three independent biological replicates of each genotype.

**UV and MMS Treatment**—*S. coelicolor* spores suspended in 20% glycerol (v/v) were filtered through 1.2- $\mu\text{m}$  filters (Sartorius) to obtain a single-spore suspension. For testing UV sensitivity, 10 ml of single-spore suspension in 20% glycerol (v/v) was poured into a 9-cm glass Petri dish and irradiated with a constant dose of UV light (50 J m<sup>-2</sup>) six times using Philips 30 W (254 nm) low pressure mercury lamp. The dose was measured by VLX-3 W radiometer. The samples were taken after each dose of irradiation, and the total dose was calculated as the sum of all received doses. For testing MMS sensitivity, raising volumes (from 0.1 to 1% (v/v)) of MMS stock solution (1.3 g/ml; Sigma) were added to the aliquots of spores suspension and incubated at 30 °C for 30 min. The reactions were terminated by diluting the spores 1:10 in 0.16 M sodium thiosulfate (47). After UV irradiation and MMS treatment, serial decimal dilutions of each sample and each dose were spread on tryptic soy broth plates and incubated at 30 °C for 24–48 h. Colony forming units were counted, and survival rates were calculated. For testing deregulation of the SCO6735 gene transcription upon DNA damage, mycelium of *S. coelicolor* wild type strain was irradiated with 200 J m<sup>-2</sup>.

**Phylogenetic Analysis**—Protein sequences were obtained from NCBI non-redundant database using human macrodomain proteins (MacroD1, TARG1, and ALC1) and a bacterial type of PARG as a query (BLAST). Macrodomains were selected from the retrieved protein sequences using SMART database or manually in the case of PARG macrodomains and aligned with the MUSCLE multiple alignment tool, using default settings (59). The multiple alignment was subjected to a maximum likelihood (ML) analysis using MEGA6 (60). The model for ML analysis was selected with ProtTest3 (61) and the Akaike information criterion (62), which indicated the Whelan\_And\_Goldman model (F + G) (63). Bayesian MCMC analysis was performed in MrBayes version 3.1.2 (64). Bootstrap tests were performed with 1000 replicates. For the structure-based alignment, we used PRALINE (65).

**Protein Crystallization and Structure Determination**—For crystallization, the protein SCO6735 was concentrated up to 10 mg/ml in 25 mM Tris-HCl (pH 7.5), 50 mM NaCl, 1 mM EDTA, 1 mM DTT, and 10% (v/v) glycerol. Initial conditions were identified utilizing sitting drop vapor diffusion method at 18 °C with JCSG III crystallization suite (Qiagen). The best crystals were obtained by hanging drop vapor diffusion method by equilibrating a 1.0- $\mu\text{l}$  drop of protein mixture in a 1:1 ratio with reservoir solution containing 0.1 M Tris-HCl (pH 7.0), 0.29 M NaCl, and 1.0 M sodium citrate. Crystals grew in 5–14 days at 18 °C. Prior to flash cooling the crystals were soaked for few

**TABLE 1**  
Data collection and refinement statistics

SCO6735	
<b>Data collection</b>	
Space group	$P4_32_1$
Cell dimensions: $a, b, c$ (Å)	103.82, 103.82, 33.25
Resolution (Å)	50–1.60 (1.64–1.60)
$R_{\text{merge}}^a$	0.120 (1.18)
$R_{\text{meas}}^b$	0.128 (1.26)
$I/\sigma(I)$	11.5 (1.8)
$CC_{1/2}$	0.996 (0.670)
Completeness (%)	97.76 (89.47)
Redundancy	8.6
<b>Refinement</b>	
Resolution (Å)	46.43–1.60
No. of reflections	22860
$R_{\text{work}}^c/R_{\text{free}}^d$	0.18/0.22 (0.26/0.35)
No. of atoms	
Macromolecule	1167
Water	161
Ligand (1 ethylene glycol and 2 Na <sup>+</sup> )	6
<b>B-Factor</b>	
Macromolecule	19.31
Water	31.53
Ligand	22.53
<b>RMSD</b>	
Bond lengths (Å)	0.023
Bond angles	2.252
<b>Ramachandran statistics (%)</b>	
Most favored regions	97
Additional allowed regions	2
Outliers	1

<sup>a</sup>  $R_{\text{merge}} = \frac{\sum_{\text{hkl}} \sum_i |I_i(\text{hkl}) - \langle I(\text{hkl}) \rangle|}{\sum_{\text{hkl}} \sum_i I_i(\text{hkl})}$ , where  $I_i(\text{hkl})$  is the intensity of a given reflection, and  $\langle I(\text{hkl}) \rangle$  is the mean intensity of symmetry-related reflections.

<sup>b</sup>  $R_{\text{meas}} = \frac{\sum_{\text{hkl}} \sqrt{n(n-1)} \sum_{i=1}^n |I_{\text{hkl},i} - \langle I_{\text{hkl}} \rangle|}{\sum_{\text{hkl}} \sum_j I_{\text{hkl},j}}$ , where  $n$  is multiplicity.  $R_{\text{meas}}$  is redundancy-independent version of  $R_{\text{merge}}$ .

<sup>c</sup>  $R_{\text{work}} = \frac{\sum_{\text{hkl}} |F_{\text{obs}} - F_{\text{calc}}|}{\sum_{\text{hkl}} F_{\text{obs}}}$ , where  $F_{\text{obs}}$  and  $F_{\text{calc}}$  are the observed and calculated structure factors, respectively.

<sup>d</sup>  $R_{\text{free}}$  was calculated using 5% of the data set chosen at random that was excluded from the refinement.

seconds in the reservoir solution containing 20% ethylene glycol as additional cryoprotectant. The crystals contain one macromolecule in the asymmetric unit corresponding to  $V_m = 9.85 \text{ \AA}^3 \text{ Da}^{-1}$  and solvent content of 52.25%.

Single crystal x-ray data collection was done on Dectris Pilatus 2M area detector at Elettra Sincrotrone Trieste, Beamline 5.2R (Table 1). Data processing was performed with XDS (66), and data scaling was performed with Aimless (67) within CCP4 (68) software suite. The structure was determined by molecular replacement with program MOLREP (69), using unknown protein from *B. thetaiotaomicron* as a model (PDB code 2FG1) obtained by Phyre2 (70). Initial model was improved by several cycles of refinement, using programs REFMAC (71, 72) and Phenix (73). Data collection and refinement statistics are given in Table 1. Final coordinates and structure factors have been deposited in the Protein Data Bank (accession number 5E3B).

**SCO6735 Activity Assay**—To test the hydrolytic activity of SCO6735, de-ADP-ribosylation assay was performed using mono-ADP-ribosylated SCO5461 $\Delta$ N34 and human PARP1 E988Q mono-mutant (performing only mono-ADP-ribosylation (7)) as substrates. Auto-ADP-ribosylation of SCO5461 $\Delta$ N34 substrate was performed in the assay buffer (50 mM Tris-HCl, pH 7.5, 50 mM NaCl, 2 mM MgCl<sub>2</sub>) at room temperature using a mixture of cold NAD<sup>+</sup> (5  $\mu\text{M}$ ) and [<sup>32</sup>P]NAD<sup>+</sup> (2  $\mu\text{Ci}$  per reaction) (PerkinElmer Life Sciences). After 30 min, the reactions were split in two, and SCO6735 was added to one aliquot at 5  $\mu\text{M}$  concentration and incubated for additional 30 min. Auto-

## References

- ADP-ribosylation of PARP1 E988Q mono-mutant was performed as previously described (55, 74), using 0.5  $\mu\text{M}$  of recombinant PARP1 E988Q. After 30 min, reaction were split and treated or not with 1  $\mu\text{M}$  of SCO6735 or SCO6735 G128E mutant. The reactions were stopped by adding SDS-PAGE loading buffer and denatured at 80 °C for 5 min. The reaction products were analyzed by SDS-PAGE and visualized by autoradiography. Quantification of residual radioactive signal on PARP1 E988Q upon treatment with SCO6735 and SCO6735 G128E mutant was performed by ImageJ, normalizing the intensity of autoradiography gel bands for the intensity of corresponding bands visualized on Coomassie staining.
- Thin Layer Chromatography**—To assess the release of [ $^{32}\text{P}$ ]ADP-ribose upon treatment with SCO6735, we used recombinant GST-PARP10cd as a substrate. GST-PARP10cd was auto-modified on beads in PARP10 reaction buffer in the presence of cold  $\text{NAD}^+$  (50  $\mu\text{M}$ ) and [ $^{32}\text{P}$ ] $\text{NAD}^+$  (2  $\mu\text{Ci}$ /reaction) for 15 min at 37 °C with continuous agitation. After incubation, beads containing GST-PARP10cd were pelleted, washed five times in reaction buffer, and split in two, and SCO6735 was added to one aliquot at 1  $\mu\text{M}$  concentration and incubated for additional 30 min. The beads were pelleted again, and 1  $\mu\text{l}$  of the liquid was phase-loaded on the thin layer chromatography plate (TLC; Macherey-Nagel, Polygram CEL 300 PEI/UV254). As [ $^{32}\text{P}$ ]ADP-ribose marker, PARP1 (Trevigen) was automodified, passed three times through G25 columns (GE Healthcare), and treated with recombinant PARG as previously described (55, 74). The plates were developed in 0.15 M LiCl and 0.15 M formic acid. Dried plates were exposed on x-ray film (55, 74).
- Mass Spectrometry Analysis**—Auto-ADP-ribosylation of SCO5461 $\Delta$ N34 protein (12.5  $\mu\text{M}$ ) was performed in the assay buffer (50 mM Tris-HCl, pH 7.5, 50 mM NaCl, 2 mM  $\text{MgCl}_2$ ) with  $\text{NAD}^+$  (50  $\mu\text{M}$ ) at room temperature for 30 min. Proteins were digested with trypsin according to the FASP protocol (75) with a 10-kDa cut-off Vivacon 500 flat ultrafiltration filters (Sartorius Stedim). The resulting peptides were analyzed by UHPLC-MS/MS on an EASY-nLC 1000 liquid chromatography system (Thermo Scientific) coupled online to a Q Exactive HF orbitrap mass spectrometer (Thermo Scientific) essentially as described before (2). The data were processed with MaxQuant (76) using parameters optimized for the detection of ADP-ribosylated peptides (2).
- 
- Author Contributions**—J. L. performed actinorhodin quantification and qRT-PCR experiments; M. P. M. purified proteins and performed biochemical analysis; L. P. performed biochemical and TLC analysis; D. P. and H. Č. performed phylogenetic analysis; I. S. and M. L. performed protein crystallization and x-ray structure determination; R. Ž. performed biochemical analysis; T. C. and I. M. performed MS experiments and data analysis; B. P. performed qRT-PCR experiments; M. H. performed DNA sequencing and sequence analysis; G. J., G. B., and M. A. performed supporting studies; A. M. performed gene cloning, gene inactivation and complementation, and wrote the manuscript; and I. A. designed experiments, analyzed data, and wrote the manuscript.
- 
- Acknowledgments**—We thank Ian Gibbs-Seymour (Sir William Dunn School of Pathology, University of Oxford, Oxford, UK) and Dušica Vujaklija (Ruđer Bošković Institute, Zagreb, Croatia) for critical reading of the manuscript.
- 
1. Barkauskaite, E., Jankevicius, G., and Ahel, I. (2015) Structures and mechanisms of enzymes employed in the synthesis and degradation of PARP-dependent protein ADP-ribosylation. *Mol. Cell* **58**, 935–946
  2. Vyas, S., Matic, I., Uchima, L., Rood, J., Zaja, R., Hay, R. T., Ahel, I., and Chang, P. (2014) Family-wide analysis of poly(ADP-ribose) polymerase activity. *Nat. Commun.* **5**, 4426
  3. Gibson, B. A., and Kraus, W. L. (2012) New insights into the molecular and cellular functions of poly(ADP-ribose) and PARPs. *Nat. Rev. Mol. Cell Biol.* **13**, 411–424
  4. Corda, D., and Di Girolamo, M. (2003) Functional aspects of protein mono-ADP-ribosylation. *EMBO J.* **22**, 1953–1958
  5. Hawse, W. F., and Wolberger, C. (2009) Structure-based mechanism of ADP-ribosylation by sirtuins. *J. Biol. Chem.* **284**, 33654–33661
  6. Slade, D., Dunstan, M. S., Barkauskaite, E., Weston, R., Lafite, P., Dixon, N., Ahel, M., Leys, D., and Ahel, I. (2011) The structure and catalytic mechanism of a poly(ADP-ribose) glycohydrolase. *Nature* **477**, 616–620
  7. Sharifi, R., Morra, R., Appel, C. D., Tallis, M., Chioza, B., Jankevicius, G., Simpson, M. A., Matic, I., Ozkan, E., Golia, B., Schellenberg, M. J., Weston, R., Williams, J. G., Rossi, M. N., Galehdari, H., et al. (2013) Deficiency of terminal ADP-ribose protein glycohydrolase TARG1/C6orf130 in neurodegenerative disease. *EMBO J.* **32**, 1225–1237
  8. Jankevicius, G., Hassler, M., Golia, B., Rybin, V., Zacharias, M., Timinszky, G., and Ladurner, A. G. (2013) A family of macrodomain proteins reverses cellular mono-ADP-ribosylation. *Nat. Struct. Mol. Biol.* **20**, 508–514
  9. Rosenthal, F., Feijs, K. L., Frugier, E., Bonalli, M., Forst, A. H., Imhof, R., Winkler, H. C., Fischer, D., Cafilisch, A., Hassa, P. O., Lüscher, B., and Hottiger, M. O. (2013) Macrodomain-containing proteins are new mono-ADP-ribosylhydrolases. *Nat. Struct. Mol. Biol.* **20**, 502–507
  10. Perina, D., Mikoč, A., Ahel, J., Četković, H. T., Žaja, R., and Ahel, I. (2014) Distribution of protein poly(ADP-ribosylation) systems across all domains of life. *DNA Repair* **23**, 4–16
  11. Till, S., and Ladurner, A. G. (2009) Sensing NAD metabolites through macro domains. *Front. Biosci.* **14**, 3246–3258
  12. Rack, J. G., Perina, D., and Ahel, I. (2016) Macrodomains: structure, function, evolution, and catalytic activities. *Annu. Rev. Biochem.* **85**, 2.1–2.24
  13. Takada, T., Iida, K., and Moss, J. (1993) Cloning and site-directed mutagenesis of human ADP-ribosylarginine hydrolase. *J. Biol. Chem.* **268**, 17837–17843
  14. Koh, D. W., Lawler, A. M., Poitras, M. F., Sasaki, M., Wattler, S., Nehls, M. C., Stöger, T., Poirier, G. G., Dawson, V. L., and Dawson, T. M. (2004) Failure to degrade poly(ADP-ribose) causes increased sensitivity to cytotoxicity and early embryonic lethality. *Proc. Natl. Acad. Sci. U.S.A.* **101**, 17699–17704
  15. Feijs, K. L., Forst, A. H., Verheugd, P., and Luscher, B. (2013) Macrodomain-containing proteins: regulating new intracellular functions of mono(ADP-ribosylation). *Nat. Rev. Mol. Cell Biol.* **14**, 542–542
  16. Holbourn, K. P., Shone, C. C., and Acharya, K. R. (2006) A family of killer toxins: exploring the mechanism of ADP-ribosylating toxins. *FEBS J.* **273**, 4579–4593
  17. Moure, V. R., Costa, F. F., Cruz, L. M., Pedrosa, F. O., Souza, E. M., Li, X. D., Winkler, F., and Huergo, L. F. (2015) Regulation of nitrogenase by reversible mono-ADP-ribosylation. *Curr. Top. Microbiol. Immunol.* **384**, 89–106
  18. Eastman, D., and Dworkin, M. (1994) Endogenous ADP-ribosylation during development of the prokaryote *Myxococcus xanthus*. *Microbiology* **140**, 3167–3176
  19. Hildebrandt, K., Eastman, D., and Dworkin, M. (1997) ADP-ribosylation by the extracellular fibrils of *Myxococcus xanthus*. *Mol. Microbiol.* **23**, 231–235
  20. Serres, M. H., and Ensign, J. C. (1996) Endogenous ADP-ribosylation of proteins in *Mycobacterium smegmatis*. *J. Bacteriol.* **178**, 6074–6077
  21. Huh, J. W., Shima, J., and Ochi, K. (1996) ADP-ribosylation of proteins in *Bacillus subtilis* and its possible importance in sporulation. *J. Bacteriol.* **178**, 4935–4941

## S. coelicolor Macrodomain Protein SCO6735

22. Ochi, K., Penyige, A., and Barabas, G. (1992) The possible role of ADP-ribosylation in sporulation and streptomycin production by *Streptomyces griseus*. *J. Gen. Microbiol.* **138**, 1745–1750
23. Penyige, A., Deák, E., Kálmánchelyi, A., and Barabás, G. (1996) Evidence of a role for NAD<sup>+</sup>-glycohydrolase and ADP-ribosyltransferase in growth and differentiation of *Streptomyces griseus* NRRL B-2682: inhibition by m-aminophenylboronic acid. *Microbiology* **142**, 1937–1944
24. Shima, J., Penyige, A., and Ochi, K. (1996) Changes in patterns of ADP-ribosylated proteins during differentiation of *Streptomyces coelicolor* A3(2) and its developmental mutants. *J. Bacteriol.* **178**, 3785–3790
25. Penyige, A., Keseru, J., Fazakas, F., Schmelczler, I., Szirák, K., Barabás, G., and Biró, S. (2009) Analysis and identification of ADP-ribosylated proteins of *Streptomyces coelicolor* M145. *J. Microbiol.* **47**, 549–556
26. Penyige, A., Vargha, G., Ensign, J. C., and Barabás, G. (1992) The possible role of ADP ribosylation in physiological regulation of sporulation in *Streptomyces griseus*. *Gene* **115**, 181–185
27. Pallen, M. J., Lam, A. C., Loman, N. J., and McBride, A. (2001) An abundance of bacterial ADP-ribosyltransferases: implications for the origin of exotoxins and their human homologues. *Trends Microbiol.* **9**, 302–307
28. Nakano, T., Matsushima-Hibiya, Y., Yamamoto, M., Takahashi-Nakaguchi, A., Fukuda, H., Ono, M., Takamura-Enya, T., Kinashi, H., and Tot-suka, Y. (2013) ADP-ribosylation of guanosine by SCO5461 protein secreted from *Streptomyces coelicolor*. *Toxicon* **63**, 55–63
29. Ahel, D., Horejsi, Z., Wiechens, N., Polo, S. E., Garcia-Wilson, E., Ahel, I., Flynn, H., Skehel, M., West, S. C., Jackson, S. P., Owen-Hughes, T., and Boulton, S. J. (2009) Poly(ADP-ribose)-dependent regulation of DNA repair by the chromatin remodeling enzyme ALC1. *Science* **325**, 1240–1243
30. Krissinel, E., and Henrick, K. (2004) Secondary-structure matching (SSM), a new tool for fast protein structure alignment in three dimensions. *Acta Crystallogr. D* **60**, 2256–2268
31. Peterson, F. C., Chen, D., Lytle, B. L., Rossi, M. N., Ahel, I., Denu, J. M., and Volkman, B. F. (2011) Orphan macrodomain protein (human C6orf130) is an O-acyl-ADP-ribose deacylase: solution structure and catalytic properties. *J. Biol. Chem.* **286**, 35955–35965
32. Ahel, I., Vujaklija, D., Mikoc, A., and Gamulin, V. (2002) Transcriptional analysis of the *recA* gene in *Streptomyces rimosus*: identification of the new type of promoter. *FEMS Microbiol. Lett.* **209**, 133–137
33. Gamulin, V., Cetkovic, H., and Ahel, I. (2004) Identification of a promoter motif regulating the major DNA damage response mechanism of Mycobacterium tuberculosis. *FEMS Microbiol. Lett.* **238**, 57–63
34. Gust, B., Challis, G. L., Fowler, K., Kieser, T., and Chater, K. F. (2003) PCR-targeted *Streptomyces* gene replacement identifies a protein domain needed for biosynthesis of the sesquiterpene soil odor geosmin. *Proc. Natl. Acad. Sci. U.S.A.* **100**, 1541–1546
35. Malpartida, F., and Hopwood, D. A. (1986) Physical and genetic characterization of the gene cluster for the antibiotic actinorhodin in *Streptomyces coelicolor* A3(2). *Mol. Gen. Genet.* **205**, 66–73
36. Liu, G., Chater, K. F., Chandra, G., Niu, G., and Tan, H. (2013) Molecular regulation of antibiotic biosynthesis in *Streptomyces*. *Microbiol. Mol. Biol. Rev.* **77**, 112–143
37. Szirák, K., Keseru, J., Biró, S., Schmelczler, I., Barabás, G., and Penyige, A. (2012) Disruption of SCO5461 gene coding for a mono-ADP-ribosyltransferase enzyme produces a conditional pleiotropic phenotype affecting morphological differentiation and antibiotic production in *Streptomyces coelicolor*. *J. Microbiol.* **50**, 409–418
38. Barkauskaite, E., Jankevicius, G., Ladurner, A. G., Ahel, I., and Timinszky, G. (2013) The recognition and removal of cellular poly(ADP-ribose) signals. *FEBS J.* **280**, 3491–3507
39. Liu, Y., Zhou, J., Omelchenko, M. V., Beliaev, A. S., Venkateswaran, A., Stair, J., Wu, L., Thompson, D. K., Xu, D., Rogozin, I. B., Gaidamakova, E. K., Zhai, M., Makarova, K. S., Koonin, E. V., and Daly, M. J. (2003) Transcriptome dynamics of *Deinococcus radiodurans* recovering from ionizing radiation. *Proc. Natl. Acad. Sci. U.S.A.* **100**, 4191–4196
40. Kim, T., Lee, J., and Kim, K. S. (2013) *Escherichia coli* YmdB regulates biofilm formation independently of its role as an RNase III modulator. *BMC Microbiol.* **13**, 266
41. Sugawara, K., Dohmae, N., Kasai, K., Saido-Sakanaka, H., Okamoto, S., Takio, K., and Ochi, K. (2002) Isolation and identification of novel ADP-ribosylated proteins from *Streptomyces coelicolor* A3(2). *Biosci. Biotechnol. Biochem.* **66**, 2292–2296
42. Aguiar, R. C., Takeyama, K., He, C., Kreinbrink, K., and Shipp, M. A. (2005) B-aggressive lymphoma family proteins have unique domains that modulate transcription and exhibit poly(ADP-ribose) polymerase activity. *J. Biol. Chem.* **280**, 33756–33765
43. Kustatscher, G., Hothorn, M., Pugieux, C., Scheffzek, K., and Ladurner, A. G. (2005) Splicing regulates NAD metabolite binding to histone macroH2A. *Nat. Struct. Mol. Biol.* **12**, 624–625
44. Tallis, M., Morra, R., Barkauskaite, E., and Ahel, I. (2014) Poly(ADP-ribose)ylation in regulation of chromatin structure and the DNA damage response. *Chromosoma* **123**, 79–90
45. Golia, B., Singh, H. R., and Timinszky, G. (2015) Poly-ADP-ribosylation signaling during DNA damage repair. *Front. Biosci. (Landmark)* **20**, 440–457
46. Stallings, C. L., Chu, L., Li, L. X., and Glickman, M. S. (2011) Catalytic and non-catalytic roles for the mono-ADP-ribosyltransferase Arr in the mycobacterial DNA damage response. *PLoS One* **6**, e21807
47. Stonesifer, J., and Baltz, R. H. (1985) Mutagenic DNA repair in *Streptomyces*. *Proc. Natl. Acad. Sci. U.S.A.* **82**, 1180–1183
48. Baltz, R. H., and Stonesifer, J. (1985) Mutagenic and error-free DNA repair in *Streptomyces*. *Mol. Gen. Genet.* **200**, 351–355
49. Kieser, T., Bibb, M. J., Buttner, M. J., Chater, K. F., and Hopwood, D. A. (2000) *Practical Streptomyces Genetics*, John Innes Foundation, Norwich, UK
50. Pigac, J., and Schrempf, H. (1995) A simple and rapid method of transformation of *Streptomyces rimosus* R6 and other streptomycetes by electroporation. *Appl. Environ. Microbiol.* **61**, 352–356
51. Redenbach, M., Kieser, H. M., Denapaite, D., Eichner, A., Cullum, J., Kinashi, H., and Hopwood, D. A. (1996) A set of ordered cosmids and a detailed genetic and physical map for the 8 Mb *Streptomyces coelicolor* A3(2) chromosome. *Mol. Microbiol.* **21**, 77–96
52. Gregory, M. A., Till, R., and Smith, M. C. (2003) Integration site for *Streptomyces* phage phi BT1 and development of site-specific integrating vectors. *J. Bacteriol.* **185**, 5320–5323
53. Xiao, Y. H., and Pei, Y. (2011) Asymmetric overlap extension PCR method for site-directed mutagenesis. *Methods Mol. Biol.* **687**, 277–282
54. Lambrecht, M. J., Brichacek, M., Barkauskaite, E., Ariza, A., Ahel, I., and Hergenrother, P. J. (2015) Synthesis of dimeric ADP-ribose and its structure with human poly(ADP-ribose) glycohydrolase. *J. Am. Chem. Soc.* **137**, 3558–3564
55. Palazzo, L., Daniels, C. M., Nettleship, J. E., Rahman, N., McPherson, R. L., Ong, S. E., Kato, K., Nureki, O., Leung, A. K., and Ahel, I. (2016) ENPP1 processes protein ADP-ribosylation *in vitro*. *FEBS J.* **10.1111/febs.13811**
56. Coze, F., Gilard, F., Tcherkez, G., Virolle, M. J., and Guyonvarch, A. (2013) Carbon-flux distribution within *Streptomyces coelicolor* metabolism: a comparison between the actinorhodin-producing strain M145 and its non-producing derivative M1146. *PLoS One* **8**, e84151
57. Pfaffl, M. W. (2004) Quantification strategies in real-time PCR. In *A–Z of quantitative PCR* (Bustin, S. A., ed) pp. 87–112, International University Line, La Jolla, CA
58. Simon, P. (2003) Q-Gen: processing quantitative real-time RT-PCR data. *Bioinformatics* **19**, 1439–1440
59. Edgar, R. C. (2004) MUSCLE: multiple sequence alignment with high accuracy and high throughput. *Nucleic Acids Res.* **32**, 1792–1797
60. Tamura, K., Stecher, G., Peterson, D., Filipiński, A., and Kumar, S. (2013) MEGA6: molecular evolutionary genetics analysis version 6.0. *Mol. Biol. Evol.* **30**, 2725–2729
61. Abascal, F., Zardoya, R., and Posada, D. (2005) ProtTest: selection of best-fit models of protein evolution. *Bioinformatics* **21**, 2104–2105
62. Posada, D., and Crandall, K. A. (1998) MODELTEST: testing the model of DNA substitution. *Bioinformatics* **14**, 817–818
63. Whelan, S., and Goldman, N. (2001) A general empirical model of protein evolution derived from multiple protein families using a maximum-likelihood approach. *Mol. Biol. Evol.* **18**, 691–699

64. Ronquist, F., and Huelsenbeck, J. P. (2003) MrBayes 3: Bayesian phylogenetic inference under mixed models. *Bioinformatics* **19**, 1572–1574
65. Simossis, V. A., and Heringa, J. (2005) PRALINE: a multiple sequence alignment toolbox that integrates homology-extended and secondary structure information. *Nucleic Acids Res.* **33**, W289–W294
66. Kabsch, W. (2010) XDS. *Acta Crystallogr. D Biol. Crystallogr.* **66**, 125–132
67. Evans, P. R., and Murshudov, G. N. (2013) How good are my data and what is the resolution? *Acta Crystallogr. D Biol. Crystallogr.* **69**, 1204–1214
68. Winn, M. D., Ballard, C. C., Cowtan, K. D., Dodson, E. J., Emsley, P., Evans, P. R., Keegan, R. M., Krissinel, E. B., Leslie, A. G., McCoy, A., McNicholas, S. J., Murshudov, G. N., Pannu, N. S., Potterton, E. A., Powell, H. R., *et al.* (2011) Overview of the CCP4 suite and current developments. *Acta Crystallogr. D Biol. Crystallogr.* **67**, 235–242
69. Vagin, A., and Teplyakov, A. (1997) MOLREP: an automated program for molecular replacement. *J. Appl. Crystallogr.* **30**, 1022–1025
70. Kelley, L. A., Mezulis, S., Yates, C. M., Wass, M. N., and Sternberg, M. J. (2015) The Phyre2 web portal for protein modeling, prediction and analysis. *Nat. Protoc.* **10**, 845–858
71. Murshudov, G. N., Skubák, P., Lebedev, A. A., Pannu, N. S., Steiner, R. A., Nicholls, R. A., Winn, M. D., Long, F., and Vagin, A. A. (2011) REFMAC5 for the refinement of macromolecular crystal structures. *Acta Crystallogr. D Biol. Crystallogr.* **67**, 355–367
72. Murshudov, G. N., Vagin, A. A., and Dodson, E. J. (1997) Refinement of macromolecular structures by the maximum-likelihood method. *Acta Crystallogr. D Biol. Crystallogr.* **53**, 240–255
73. Adams, P. D., Afonine, P. V., Bunkóczi, G., Chen, V. B., Davis, I. W., Echols, N., Headd, J. J., Hung, L. W., Kapral, G. J., Grosse-Kunstleve, R. W., McCoy, A. J., Moriarty, N. W., Oeffner, R., Read, R. J., Richardson, D. C., *et al.* (2010) PHENIX: a comprehensive Python-based system for macromolecular structure solution. *Acta Crystallogr. D Biol. Crystallogr.* **66**, 213–221
74. Palazzo, L., Thomas, B., Jemth, A. S., Colby, T., Leidecker, O., Feijs, K. L., Zaja, R., Loseva, O., Puigvert, J. C., Matic, I., Helleday, T., and Ahel, I. (2015) Processing of protein ADP-ribosylation by Nudix hydrolases. *Biochem. J.* **468**, 293–301
75. Wiśniewski, J. R., Zougman, A., Nagaraj, N., and Mann, M. (2009) Universal sample preparation method for proteome analysis. *Nat. Methods* **6**, 359–362
76. Cox, J., and Mann, M. (2008) MaxQuant enables high peptide identification rates, individualized p.p.b.-range mass accuracies and proteome-wide protein quantification. *Nat. Biotechnol.* **26**, 1367–1372